Reduction–Oxidation Properties of Organotransition-metal Complexes. Part 22.[1] Stereospecific Oxidative Cyclopropane Ring Opening and Reductive Cyclobutane Ring Formation in Polycyclic Hydrocarbon Complexes of Iron; *X*-Ray Crystal Structures of $[Fe_2(CO)_6(\eta^5:\eta'^5\text{-}C_{16}H_{16})][PF_6]_2\cdot CH_3NO_2$ and $[Fe_2(CO)_6(\eta^4:\eta'^4\text{-}C_{16}H_{16})]$ *

Neil G. Connelly, Mark J. Freeman, A. Guy Orpen, John B. Sheridan, Andrew N. D. Symonds, and Mark W. Whiteley
Department of Inorganic Chemistry, University of Bristol, Bristol BS8 1TS

Electrochemical studies show that $[Fe_2(CO)_6(\eta^4:\eta'^4\text{-}C_{16}H_{16})]$ (**2**) undergoes irreversible two-electron oxidation at a platinum electrode in CH_2Cl_2. Chemical oxidation with $[Fe(\eta\text{-}C_5H_5)_2][PF_6]$ gives $[Fe_2(CO)_6(\eta^5:\eta'^5\text{-}C_{16}H_{16})][PF_6]_2$ (**3**), *X*-ray structural studies on the nitromethane solvate of which reveal the detailed stereochemistry of the polycyclic hydrocarbon ligand. Two cycloheptadienyl moieties, each η^5-bonded to $Fe(CO)_3$ units, are fused to a central cyclohexene ring at C(2)–C(3) and at C(2')–C(3'). The six-membered ring adopts a very flattened chair conformation with C(4) and C(4') (bonded to iron as terminal members of pentadienyl units) in pseudo-axial sites, at 3.78 Å apart. Complex (**3**) is reduced by $K[BH(CHMeEt)_3]$ to $[Fe_2(CO)_6(\eta^4:\eta'^4\text{-}C_{16}H_{16})]$ (**4**), *X*-ray structural studies on which show stereospecific cyclobutane ring formation *via* the linking of atoms C(4) and C(4') of (**3**). This linking is accompanied by ring inversion of the cyclohexene residue and by significant twisting of the ring double bond [C(2)–C(1)–C(1')–C(2') torsion angle −8.6(5)°]. The C(4)–C(4') bond formed is the longest in the cyclobutane ring at 1.596(4) Å [*cf.* others, average 1.548(3) Å]. The ring inversion is required to bring C(4) and C(4') into adjacent pseudo-equatorial sites and hence proximity [the C(4)–C(3)–C(3')–C(4') torsion angle is 159.7(4)° in (**3**) and 25.2(2)° in (**4**)]. Complex (**4**) is oxidised by $[Fe(\eta\text{-}C_5H_5)_2][PF_6]$ to (**3**) which reacts with PPh_3 and with iodide ion to give $[Fe_2(CO)_6\{\eta^4:\eta'^4\text{-}C_{16}H_{16}(PPh_3)_2\}][PF_6]_2$ (**5**) and $[Fe_2I_2(CO)_4(\eta^5:\eta'^5\text{-}C_{16}H_{16})]$ (**6**), respectively.

We have recently described[2] the stereospecific oxidative cyclopropane ring-opening reaction of $[Fe_2(CO)_6(\eta^4:\eta'^4\text{-}C_{16}H_{18})]$, which generates a *trans*-olefinic double bond in the dicationic product $[Fe_2(CO)_6(\eta^5:\eta'^5\text{-}C_{16}H_{18})]^{2+}$. We now report details[3] of the related reaction of $[Fe_2(CO)_6(\eta^4:\eta'^4\text{-}C_{16}H_{16})]$ (**2**) (Scheme) to give $[Fe_2(CO)_6(\eta^5:\eta'^5\text{-}C_{16}H_{16})]^{2+}$ (**3**) the hydrocarbon ligand of which consists of a cyclohexene ring fused to two cycloheptadienyl units. The reduction of (**3**) yields $[Fe_2(CO)_6(\eta^4:\eta'^4\text{-}C_{16}H_{16})]$ (**4**) in which C–C bond formation generates a cyclobutane ring. *X*-Ray structural studies on (**3**) and (**4**), in comparison with those on $[Fe_2(CO)_4L_2(\eta^5:\eta'^5\text{-}C_{16}H_{16})]^{2+}$ [**1**; L = $P(OPh)_3$][4] and (**2**),[5] provide an insight into the origin of the observed stereospecificity of the redox reactions. The reactions of (**3**) with nucleophiles are also reported briefly.

Results and Discussion

Synthetic and Structural Studies.—The complex $[Fe_2(CO)_6(\eta^4:\eta'^4\text{-}C_{16}H_{16})]$ (**2**) (Scheme), previously prepared[2] by sequentially reacting $[Fe_2(CO)_6(\eta^5:\eta'^5\text{-}C_{16}H_{16})]^{2+}$ (**1**; L = CO) with bromide ion and $[Fe_2(CO)_9]$, has now been isolated directly by reducing the dication with $K[BH(CHMeEt)_3]$. The yield is no better than that previously obtained but the one-step synthesis is more convenient.

The cyclic voltammogram of (**2**), in CH_2Cl_2 at a platinum bead electrode, shows one, diffusion-controlled ($i/v^{\frac{1}{2}}$ = constant for scan rates, v, from 50 to 500 mV s^{-1}) but irreversible oxidation wave with a peak potential of 0.87 V [*vs.* a saturated calomel electrode (s.c.e.) at a scan rate of 200 mV s^{-1}]. The peak current is approximately twice that of $[Fe(CO)_3(\eta^4\text{-cot})]$ (cot = cyclo-octatetraene), measured under identical conditions, suggesting that (**2**) is oxidised in a two-electron step. Although the insolubility of the oxidation product in CH_2Cl_2 (see below) precluded direct confirmation of the number of electrons involved in the redox reaction (by controlled potential electrolysis and coulometry), chemical oxidation of (**2**) requires *two* equivalents of the one-electron oxidant $[Fe(\eta\text{-}C_5H_5)_2][PF_6]$. Thus, mixing (**2**) and the ferrocenium ion in CH_2Cl_2 readily gives good yields of $[Fe_2(CO)_6(\eta^5:\eta'^5\text{-}C_{16}H_{16})][PF_6]_2$ (**3**) as a pale yellow precipitate. Despite the apparently unfavourable potentials for the oxidation of (**2**) and the reduction of $[Fe(\eta\text{-}C_5H_5)_2]^+$ (0.48 V), the reaction proceeds because of the irreversible chemical formation of (**3**).

Chemical reduction of (**3**), by $K[BH(CHMeEt)_3]$ in tetrahydrofuran (thf) at −78 °C, gave an orange solution from which a low yield of yellow, crystalline $[Fe_2(CO)_6(\eta^4:\eta'^4\text{-}C_{16}H_{16})]$ (**4**) was isolated by column chromatography. Complexes (**3**) and (**4**) were characterised by elemental analysis and i.r. spectroscopy (Table 1), and by ^1H and ^{13}C n.m.r. spectroscopy (Table 2) which revealed the basic arrangements of the hydrocarbon skeletons (Scheme). The detailed molecular geometries were, however, only fully established by *X*-ray crystallography.

The crystal structures of (**3**)·CH_3NO_2 and (**4**) were

* μ-(1—5-η:8—12-η'-1,5a,7a,12,12a,12b-Hexahydrobenzo[*a*,*c*]-dicycloheptenyl)-bis(tricarbonyliron) hexafluorophosphate–nitromethane (1/1) and μ-(2—5-η:6—9-η'-1,10-etheno-1,5a,5b,10,10a,10b-hexahydrocyclobuta[1,2:3,4]dicycloheptene)-bis(tricarbonyliron).

Supplementary data available (No. SUP 56183, 9 pp.): isotropic and anisotropic thermal parameters, H-atom co-ordinates. See Instructions for Authors, *J. Chem. Soc., Dalton Trans.*, 1985, Issue 1, pp. xvii–xix. Structure factors are available from the editorial office.

Table 1. Infrared spectral and analytical data

Complex	Yield (%)	M.p. (θ_c/°C)	ν(CO)/cm^{-1}	Analysis[a] (%) C	H	N
(3) $[Fe_2(CO)_6(\eta^5:\eta'^5\text{-}C_{16}H_{16})][PF_6]_2\cdot CH_3NO_2$	94		2 119, 2 075[b]	32.6 (32.9)	2.2 (2.3)	1.7 (1.7)
(4) $[Fe_2(CO)_6(\eta^4:\eta'^4\text{-}C_{16}H_{16})]$	20	Decomp. >85	2 044, 1 981, 1 977[c]	54.3 (54.1)	3.4 (3.3)	—
(5) $[Fe_2(CO)_6\{\eta^4:\eta'^4\text{-}C_{16}H_{16}(PPh_3)_2\}][PF_6]_2\cdot CH_2Cl_2$	72	195—200	2 055, 1 991, 1 981[d]	51.0 (51.0)	3.7 (3.5)[e]	—
(6) $[Fe_2I_2(CO)_4(\eta^5:\eta'^5\text{-}C_{16}H_{16})]$	52		2 027, 1 991[d]	35.1 (34.9)	2.5 (2.6)	—

[a] Calculated values are given in parentheses. [b] In Nujol. [c] In n-hexane. [d] In CH_2Cl_2. [e] Calculated values include one molecule of CH_2Cl_2 of crystallisation.

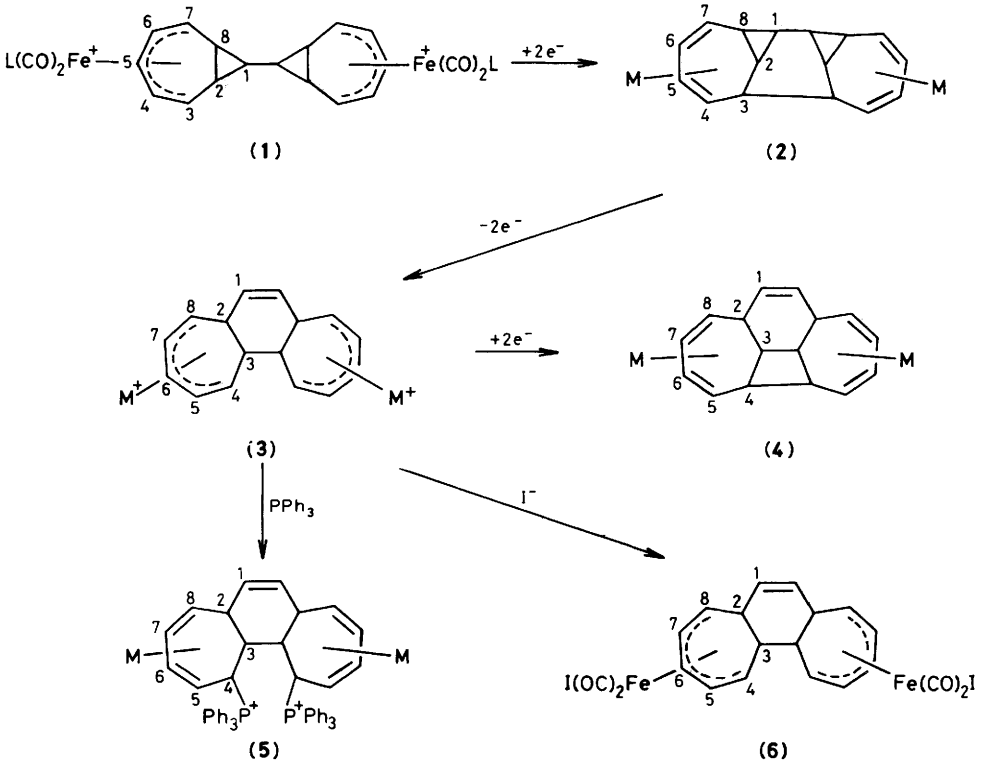

Scheme. M = $Fe(CO)_3$, L = CO or $P(OPh)_3$

determined by room-temperature single-crystal *X*-ray diffraction studies, full details of which are given in the Experimental section below. Selected derived bond lengths and angles for (**3**) and (**4**) are listed in Tables 3 and 4; Table 5 summarises important torsion angles within the $C_{16}H_{16}$ skeletons. Figures 1 and 2 show the non-hydrogen frameworks of (**3**) and (**4**), respectively, with the atomic labelling scheme adopted.

The dication of (**3**) (Figure 1) contains a tricyclic $C_{16}H_{16}$ moiety comprising a cyclohexene ring [C(1), C(2), C(3), C(1′), C(2′), C(3′)] fused to two cycloheptadienyl residues at C(2)–C(3) and C(2′)–C(3′); the seven-membered rings are each η^5-bonded to $Fe(CO)_3$ units. The dication as a whole has rather approximate (non-crystallographic) C_2 symmetry, the primed atoms being related to those not primed by this 'symmetry'. Inspection of Table 5 shows that the corresponding C–C–C–C torsion angles in related parts of the molecule differ significantly, by up to *ca.* 13.9° (> 20σ).

The heptadienyl units consist of a planar dienyl fragment, C(4)–C(5)–C(6)–C(7)–C(8) (r.m.s. deviation 0.04 [0.04] Å *), and a second planar four-carbon fragment C(8)–C(2)–C(3)–C(4) (r.m.s. deviation 0.012 [0.017] Å). The ring is therefore folded about the C(4) • • • C(8) axis, with an interplanar angle of 46 [46]°. Less pronounced but similar folding was noted in $[Fe_2(CO)_4\{P(OPh)_3\}_2(\eta^5:\eta'^5\text{-}C_{16}H_{16})]^{2+}$ [**1**; L = $P(OPh)_3$][4] where the corresponding dihedral angle was 36°. The carbonyl ligands are quite normal being near linear and with OC–Fe–CO angles near 90°. The $Fe(CO)_3$ fragment adopts the ground-state conformation as in structure (**A**), this being that favoured on electronic grounds [6] and observed in numerous ML_3(dienyl) complexes, *e.g.* [**1**; L = $P(OPh)_3$].[4] As in the latter complexes the iron–dienyl carbon distances vary, with the longest from the metal to the terminal atoms [C(4), C(4′), C(8), C(8′)] [av. 2.184(6) Å;† *cf.* others, av. 2.096(6) Å]. The dienyl C–C dis-

* Values for primed atoms are given in square brackets where applicable.

† Estimated standard deviations in the least significant digit are given in parentheses here and throughout this paper.

Table 2. Proton and ^{13}C n.m.r. spectral data[a]

Compound	^1H (δ)[b]	^{13}C (p.p.m.)[c]
(3)·CH_3NO_2	3.11 [1 H, dd, $J(H^3H^4)$ 7, H^3], 3.50 [1 H, m, $J(H^2H^3)$ 8, H^2], 4.95 [1 H, m, $J(H^8H^2)$ 3.5, $J(H^8H^7)$ 10, H^8], 5.01 (1 H, s, H^1), 5.19 [1 H, dd, $J(H^4H^5)$ 8, $J(H^4H^3)$ 7, H^4], 5.96 [1 H, dd, $J(H^7H^8)$ 10, H^7], 6.16 [1 H, dd, $J(H^5H^6)$ 6, $J(H^5H^4)$ 8, H^5], 7.11 [1 H, dd, $J(H^6H^7)$ 8, $J(H^6H^5)$ 6, H^6][d]	35.7 (C^3), 55.5 (C^2), 91.2, 94.5 (C^4, C^8), 101.3, 104.6 (C^5, C^7), 103.3 (C^6), 127.7 (C^1), 202.0 (CO)[d]
(4)	2.05 [1 H, m,br, H^3], 2.51 [2 H, m, H^2, H^4], 3.03 [1 H, dd, $J(H^8H^2)$ 3, $J(H^8H^7)$ 9, H^8], 3.22 [1 H, dd, $J(H^5H^4)$ 4.5, $J(H^5H^6)$ 9, H^5], 5.32 [2 H, m, H^6, H^7], 5.63 [1 H, quartet,[e] $J(H^1H^{1'})$ 9.5, $J(H^1H^2)$ 4.5, $J(H^1H^{2'})$ −2.3, H^1][f]	31.8 (C^3), 36.5 (C^4), 47.0 (C^2), 64.2, 64.6 (C^5, C^8), 88.6 (C^6, C^7), 133.4 (C^1), 211.3 (CO)[f]
(5)·CH_2Cl_2	2.68 [1 H, d, $J(H^8H^7)$ 8, H^8], 2.74 (1 H, s,br, H^2), 3.27 [1 H, dd, $J(H^5H^6)$ 7, $J(H^5P)$ 16, H^5], 3.42 (1 H, m, H^3), 4.70 [1 H, dd, $J(H^4H^3)$ 2, $J(H^4P)$ 20.5, H^4], 5.56 (2 H, m, H^1,H^7), 5.98 [1 H, dd, $J(H^6H^7)$ 6, $J(H^6H^5)$ 7, H^6], 7.90 (15 H, m, PPh_3)[g]	
(6)	2.56 [1 H, dd, $J(H^3H^2)$ 8, H^3], 2.87 [1 H, m, H^2], 3.80 [2 H, m, $J(H^4H^5)$, $J(H^8H^7)$ 9, H^4, H^8], 4.61 (1 H, s, H^1), 5.38 (1 H, dd, H^7), 5.54 (1 H, dd, H^5), 6.74 [1 H, dd, $J(H^6H^7)$, $J(H^6H^5)$ 6, H^6][f]	35.6 (C^3), 53.0 (C^2), 80.6 (C^4, C^8, br), 97.0 (C^6), 100.0, 101.6 (C^5,C^7, br), 126.8 (C^1)[f,h]

[a] Numbering as in the Scheme; J values in Hz. Chemical shifts are downfield from $SiMe_4$. [b] 200 MHz spectra. [c] 50 MHz spectra unless stated otherwise. [d] In CD_3NO_2. [e] $[AX]_2$ spectrum with $J(H^2H^{2'}) \approx 0$ Hz. [f] In $CDCl_3$. [g] In $(CD_3)_2CO$. [h] 22.50 MHz spectrum. One signal was obscured by the solvent.

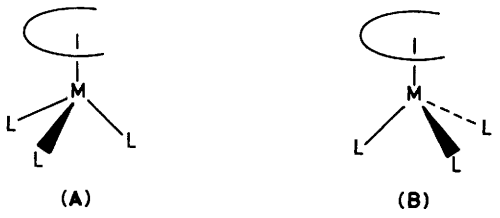

tances vary little, from 1.419(8) to 1.368(9) Å, and average 1.393(6) Å.

The cyclohexene ring conformation, as determined in the solid state, is consistent with the ^1H n.m.r. spectrum of (3). Thus, the $(AX)_2$ spectrum of H(1) is a singlet, implying $J(H^1H^2)$ is close to zero and bonds C(1)–H(1) and C(2)–H(2) are nearly orthogonal; the H(1)–C(1)–C(2)–H(2) torsion angle is 66(4) [79(5)]°.

The molecular structure of (4) (Figure 2) also shows approximate (non-crystallographic) C_2 symmetry, although rather more precisely than does (3). The largest C–C–C–C torsion angle deviation from this symmetry is 1.5° ($<4\sigma$). The hydrocarbon skeleton contains one additional, four-membered ring as compared with (3), formed by linking C(4) and C(4′). The seven-membered rings are now η^4-bonded to the $Fe(CO)_3$ units, C(4) and C(4′) having been detached from iron on reducing (3) to (4).

The seven-membered rings consist once more of two approximately planar sections, one C(5),C(6),C(7),C(8) η^4-bonded to iron (r.m.s. deviation 0.002 [0.002] Å) and the other, C(8),C(2),C(3),C(4),C(5) fused to the cyclobutane [at C(3)–C(4)] and cyclohexene [at C(2)–C(3)] rings. Here the fold along the C(5)···C(8) axis is 136 [135]°.

The bonding of the $Fe(CO)_3$ fragments to the diene portions of the C_7 rings is similar to that observed previously for $[Fe(CO)_3(\eta^4\text{-}C_7H_7CH{=}CHPh)]$[7] and the related complexes $[Fe(CO)_3(\eta^4\text{-}C_7H_7Ph)]$,[8] $[Fe(CO)_3(\eta^4\text{-}C_7H_6O)]$,[9] $[Fe(CO)_3(\eta^4\text{-}C_7H_3Ph_3O)]$,[10] $[Fe_2(CO)_6(\eta^4{:}\eta'^4\text{-}C_{16}H_{16})]$ (2),[5] $[Fe(CO)_3(\eta^4\text{-}C_{16}H_{16})]$,[4] and $[Fe_2(CO)_6(\eta^4{:}\eta'^4\text{-}C_{16}H_{18})]$.[2] Thus the 'outer' Fe–C(diene) lengths [mean for (4), 2.140(3) Å] are significantly longer than the 'inner' Fe–C distances [av. 2.055(3) Å]. The C–C diene distances indicate substantial occupancy of the diene lowest unoccupied molecular orbital (l.u.m.o.) showing a long–short–long pattern [mean for (4), C(5)–C(6) 1.427(4), C(6)–C(7) 1.392(4), C(7)–C(8) 1.423(4) Å].

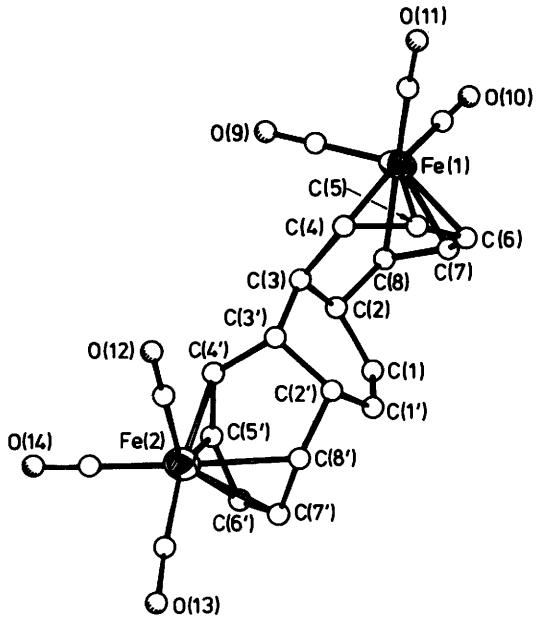

Figure 1. Molecular structure of the dication of (3) showing the atomic labelling scheme; hydrogen atoms have been omitted for clarity

The newly formed C(4)–C(4′) bond in the cyclobutane ring is clearly under strain having the longest C–C distance 1.596(4) Å [*cf.* others in the C_4 ring average 1.548(3) Å]. The moduli of torsion angles within this ring vary between 24.3(2) and 25.2(2)°, typical of a range of non-planar cyclobutanes (see ref. 11 and references therein). The conformational changes resulting from C(4)–C(4′) bond formation (discussed further below) cause a substantial reduction in the H(1)–C(1)–C(2)–H(2) torsion angle relative to that in (3), to 47(2) [48(2)]°, and hence explain the increase in the ^1H n.m.r. coupling constant $J(H^1H^2)$ of (4) (4.5 Hz).

Mechanisms of Formation of and Structural Relationships between Complexes (1)—(4).—Each of the reactions linking complexes (1)—(4) involves electron transfer followed by hydrocarbon ring rearrangement. In general terms, the reduction reactions, of (1) and (3), involve electron addition to the

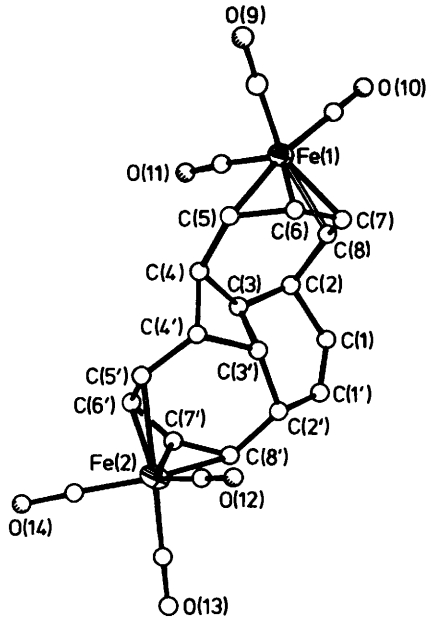

Figure 2. Molecular structure of (**4**) showing the atomic labelling scheme adopted; hydrogen atoms have been omitted for clarity

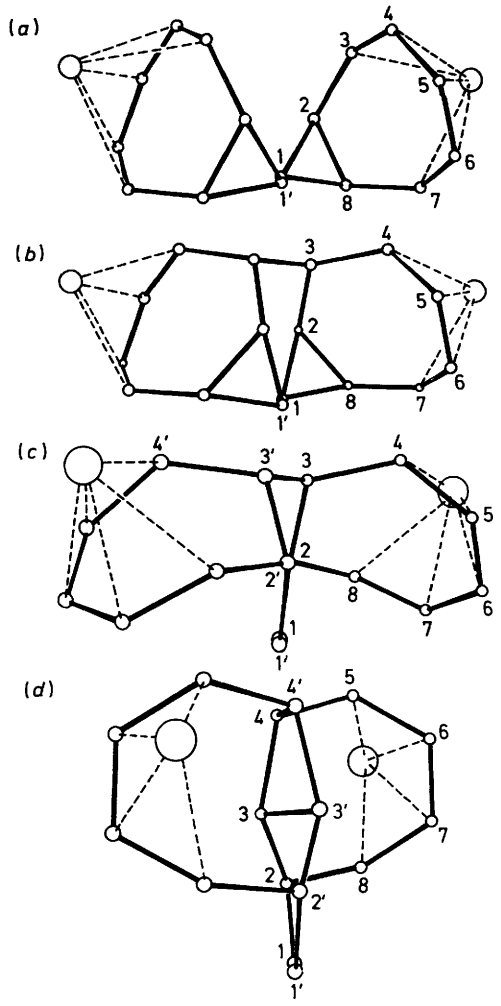

Figure 3. The Fe_2C_{16} cores of (*a*) [**1**; L = $P(OPh)_3$], (*b*) (**2**), (*c*) (**3**), and (*d*) (**4**) viewed along the C(1)–C(1′) bonds

metal atom (to give a 19-electron configuration) or to the η^5-dienyl unit, detachment of a terminal dienyl carbon from each iron to give tricarbonyl(η^4-diene)iron moieties, and radical–radical coupling between carbon atoms bearing unpaired electrons. The oxidation reactions, of (**2**) and (**4**) [the latter is quantitatively reoxidised to (**3**) on treatment with ferrocenium ion], involve electron loss from the iron centres, as described earlier for $[Fe_2(CO)_6(\eta^4:\eta'^4\text{-}C_{16}H_{18})]$.[2] Subsequent attainment of the more stable 18-electron configuration, *via* bonding of the metal to an adjacent carbon atom, results in the formation of a cationic tricarbonyl(η^5-dienyl)iron moiety.

However, more detailed information concerning the mechanisms of the reactions linking (**1**)—(**4**) is available from *X*-ray crystallographic studies, particularly with regard to the observed stereo- and regio-specificities.

Figure 3(*a*)—(*d*) illustrates the hydrocarbon skeletons of [**1**; L = $P(OPh)_3$], (**2**), (**3**), and (**4**) (with the positions of the bonded iron atoms) viewed along the bond between C(1) and C(1′). It should be noted that the conformation of [**1**; L = $P(OPh)_3$] {and the very similar conformation of $[Fe_2(CO)_6(\eta^4:\eta'^4\text{-}C_{16}H_{18})]$}[2] is somewhat rotated about C(1)–C(1′) from that which places the two bicyclo[5.1.0]octadienyl groups exactly *trans*; the dihedral angle H(1)–C(1)–C(1′)–H(1′) is *ca.* 140°, rather than 180°. This arises because of unfavourable H • • • C non-bonded contacts between H(1′) and C(4) and C(5). On rotation about C(1)–C(1′) to the *trans* orientation these contacts fall from *ca.* 2.8 Å (similar to other transannular H • • • C distances in these complexes) to less than 2.5 Å.

When (**1**) is reduced to (**2**), little conformational change is required to bring C(3) and C(3′) close enough to bond. Thus the C(3)–C(3′) separation is reduced from 3.58 Å in [**1**; L = $P(OPh)_3$] to 1.56 Å in (**2**) by rotation of the bicyclo[5.1.0]octadienyl units about the C(1)–C(1′) bond. The C(2)–C(1)–C(1′)–C(2′) torsion angle falls from 59.7° in [**1**; L = $P(OPh)_3$] to 27° in (**2**).

Subsequent carbon–carbon bond cleavage and formation in the sequence (**2**) ⟶ (**3**) ⟶ (**4**) appears to be controlled in part by the stereochemical requirements of the six-membered ring [C(1)–C(2)–C(3)–C(1′)–C(2′)–C(3′)]. Thus oxidation of (**2**) results in cleavage of the C(1)–C(8) [C(1′)–C(8′)] bonds in preference to C(3)–C(3′) [which would regenerate (**1**)]. Clearly the cyclopropane ring C–C bonds are the most strained in the hydrocarbon skeleton of (**2**) and therefore most prone to cleavage. The observed cleavage of C(1)–C(8) [C(1′)–C(8′)] allows relief of angular strain at C(2), and the formation of the Fe–C(8) [C(8′)] bonds completes co-ordinative saturation at Fe, C(8), and C(8′).

These changes cause relatively little conformational problem for the six-membered ring despite its conversion to a cyclohexene residue in (**3**) [C(1)–C(1′) 1.299(9) Å, *cf.* 1.49(2) Å in (**2**)]. However, the conformation about the C(1)–C(1′) bond undergoes a further change, in addition to that observed from [**1**; L = $P(OPh)_3$] to (**2**), in that the angle C(2)–C(1)–C(1′)–C(2′) is now reduced to 1.0(10)°.

The formation of (**3**) from (**2**) can therefore be viewed as an oxidation of the metal followed by electrophilic attack by that metal on C(8). The latter step proceeds with inversion of configuration at C(8), and with an increase of the C(1)–C(1′) bond order to two. Other possible courses following the oxidation could be envisaged, for example electrophilic attack on C(2), or attack at C(8) with cleavage of C(2)–C(8) and formation of a C(2)–C(2′) bond. These possibilities would appear to be unfavourable because of the preference of the $Fe(CO)_3$ moiety for binding to an η^5-dienyl fragment, rather than to an η^4-diene and σ-alkyl group in the former case, and in

Table 3. Bond lengths and angles for (3)·CH_3NO_2

Bond lengths (Å)

Fe(1)–C(4)	2.160(5)	Fe(1)–C(5)	2.100(6)	C(3)–C(4)	1.504(8)	C(3)–C(3′)	1.563(7)
Fe(1)–C(6)	2.095(7)	Fe(1)–C(7)	2.082(6)	C(9)–O(9)	1.132(8)	C(4)–C(5)	1.383(8)
Fe(1)–C(8)	2.195(6)	Fe(1)–C(9)	1.799(7)	C(11)–O(11)	1.123(9)	C(5)–C(6)	1.406(8)
Fe(1)–C(10)	1.828(5)	Fe(1)–C(11)	1.814(7)	C(2′)–C(8′)	1.519(8)	C(6)–C(7)	1.383(10)
Fe(2)–C(4′)	2.183(5)	Fe(2)–C(5′)	2.105(6)	C(3′)–C(4′)	1.492(7)	C(7)–C(8)	1.368(9)
Fe(2)–C(6′)	2.092(6)	Fe(2)–C(7′)	2.097(6)	C(4′)–C(5′)	1.419(8)	C(10)–O(10)	1.125(6)
Fe(2)–C(8′)	2.197(6)	Fe(2)–C(12)	1.813(7)	C(5′)–C(6′)	1.399(9)	C(1′)–C(2′)	1.502(8)
Fe(2)–C(13)	1.810(6)	Fe(2)–C(14)	1.821(6)	C(6′)–C(7′)	1.396(10)	C(2′)–C(3′)	1.506(8)
C(1)–C(2)	1.494(8)	C(1)–C(1′)	1.299(9)	C(7′)–C(8′)	1.387(8)	C(12)–O(12)	1.129(9)
C(2)–C(8)	1.533(7)	C(2)–C(3)	1.521(7)	C(13)–O(13)	1.121(8)	C(14)–O(14)	1.135(8)

Bond angles (°)

C(4)–Fe(1)–C(5)	37.9(2)	C(4)–Fe(1)–C(6)	71.3(2)	C(12)–Fe(2)–C(14)	94.0(3)	C(13)–Fe(2)–C(14)	89.5(3)
C(5)–Fe(1)–C(6)	39.2(2)	C(4)–Fe(1)–C(7)	89.3(2)	C(2)–C(1)–C(1′)	125.1(5)	C(1)–C(2)–C(3)	113.0(5)
C(5)–Fe(1)–C(7)	72.1(2)	C(6)–Fe(1)–C(7)	38.7(3)	C(1)–C(2)–C(8)	108.5(4)	C(3)–C(2)–C(8)	111.6(4)
C(4)–Fe(1)–C(8)	78.5(2)	C(5)–Fe(1)–C(8)	85.0(2)	C(2)–C(3)–C(4)	112.6(4)	C(2)–C(3)–C(3′)	113.5(4)
C(6)–Fe(1)–C(8)	68.3(3)	C(7)–Fe(1)–C(8)	37.2(2)	C(4)–C(3)–C(3′)	108.4(4)	Fe(1)–C(4)–C(3)	110.6(4)
C(4)–Fe(1)–C(9)	87.1(3)	C(5)–Fe(1)–C(9)	124.9(2)	Fe(1)–C(4)–C(5)	68.7(3)	C(3)–C(4)–C(5)	129.6(5)
C(6)–Fe(1)–C(9)	149.5(3)	C(7)–Fe(1)–C(9)	123.1(3)	Fe(1)–C(5)–C(4)	73.5(4)	Fe(1)–C(5)–C(6)	70.2(4)
C(8)–Fe(1)–C(9)	86.8(3)	C(4)–Fe(1)–C(10)	174.6(2)	C(4)–C(5)–C(6)	125.7(6)	Fe(1)–C(6)–C(5)	70.6(4)
C(5)–Fe(1)–C(10)	139.1(2)	C(6)–Fe(1)–C(10)	104.1(3)	Fe(1)–C(6)–C(7)	70.2(4)	C(5)–C(6)–C(7)	123.8(6)
C(7)–Fe(1)–C(10)	85.3(2)	C(8)–Fe(1)–C(10)	97.3(2)	Fe(1)–C(7)–C(6)	71.2(4)	Fe(1)–C(7)–C(8)	75.9(4)
C(9)–Fe(1)–C(10)	96.0(3)	C(4)–Fe(1)–C(11)	93.7(2)	C(6)–C(7)–C(8)	122.3(5)	Fe(1)–C(8)–C(2)	113.6(4)
C(5)–Fe(1)–C(11)	86.1(3)	C(6)–Fe(1)–C(11)	105.3(3)	Fe(1)–C(8)–C(7)	66.9(3)	C(2)–C(8)–C(7)	123.4(6)
C(7)–Fe(1)–C(11)	139.7(3)	C(8)–Fe(1)–C(11)	171.1(3)	Fe(1)–C(9)–O(9)	178.2(6)	Fe(1)–C(10)–O(10)	180.0(8)
C(9)–Fe(1)–C(11)	97.2(3)	C(10)–Fe(1)–C(11)	90.3(3)	Fe(1)–C(11)–O(11)	176.5(7)	C(1)–C(1′)–C(2′)	125.2(5)
C(4′)–Fe(2)–C(5′)	38.6(2)	C(4′)–Fe(2)–C(6′)	72.3(2)	C(1′)–C(2′)–C(3′)	110.5(5)	C(1′)–C(2′)–C(8′)	111.5(5)
C(5′)–Fe(2)–C(6′)	38.9(2)	C(4′)–Fe(2)–C(7′)	90.1(2)	C(3′)–C(2′)–C(8′)	110.7(4)	C(3)–C(3′)–C(2′)	113.9(4)
C(5′)–Fe(2)–C(7′)	71.7(2)	C(6′)–Fe(2)–C(7′)	38.9(3)	C(3)–C(3′)–C(4′)	110.7(5)	C(2′)–C(3′)–C(4′)	110.5(4)
C(4′)–Fe(2)–C(8′)	77.8(2)	C(5′)–Fe(2)–C(8′)	83.9(2)	Fe(2)–C(4′)–C(3′)	108.4(4)	Fe(2)–C(4′)–C(5′)	67.7(3)
C(6′)–Fe(2)–C(8′)	68.5(2)	C(7′)–Fe(2)–C(8′)	37.6(2)	C(3′)–C(4′)–C(5′)	129.7(5)	Fe(2)–C(5′)–C(4′)	73.7(3)
C(4′)–Fe(2)–C(12)	85.4(2)	C(5′)–Fe(2)–C(12)	123.7(3)	Fe(2)–C(5′)–C(6′)	70.1(3)	C(4′)–C(5′)–C(6′)	127.3(6)
C(6′)–Fe(2)–C(12)	151.8(2)	C(7′)–Fe(2)–C(12)	127.1(3)	Fe(2)–C(6′)–C(5′)	71.0(3)	Fe(2)–C(6′)–C(7′)	70.7(3)
C(8′)–Fe(2)–C(12)	90.4(3)	C(4′)–Fe(2)–C(13)	173.3(3)	C(5′)–C(6′)–C(7′)	123.5(5)	Fe(2)–C(7′)–C(6′)	70.4(3)
C(5′)–Fe(2)–C(13)	140.2(3)	C(6′)–Fe(2)–C(13)	104.1(3)	Fe(2)–C(7′)–C(8′)	75.1(3)	C(6′)–C(7′)–C(8′)	120.5(6)
C(7′)–Fe(2)–C(13)	83.8(3)	C(8′)–Fe(2)–C(13)	95.6(3)	Fe(2)–C(8′)–C(2′)	113.2(4)	Fe(2)–C(8′)–C(7′)	67.3(3)
C(12)–Fe(2)–C(13)	96.1(3)	C(4′)–Fe(2)–C(14)	96.9(2)	C(2′)–C(8′)–C(7′)	120.9(5)	Fe(2)–C(12)–O(12)	178.9(6)
C(5′)–Fe(2)–C(14)	89.0(3)	C(6′)–Fe(2)–C(14)	105.5(3)	Fe(2)–C(13)–O(13)	177.2(6)	Fe(2)–C(14)–O(14)	177.2(6)
C(7′)–Fe(2)–C(14)	138.8(3)	C(8′)–Fe(2)–C(14)	172.9(3)				

the latter because the resulting hydrocarbon ligand would contain two, strained, fused cyclobutane rings.

The final reductive coupling reaction, converting (**3**) to (**4**), requires the greatest apparent conformational change as illustrated in Figure 3. The formation of the C(4)–C(4′) bond is allowed by a dramatic change in the C(4)–C(3)–C(3′)–C(4′) torsion angle from 159.7(4)° in (**3**) to 25.2(2)° in (**4**) (where it is one of the cyclobutane intra-ring torsion angles). This change is accompanied by inversion of the cyclohexene ring conformation as illustrated by Figure 3 (see also Table 5). The effect of this inversion is to move C(4) and C(4′) from *trans* to *gauche* positions on C(3)–C(3′), *i.e.* from adjacent axial to equatorial sites on the C_6 ring as is required to reduce C(4) · · · C(4′) to a bonding distance.

The conformational pressure within the six-membered ring, caused by the formation of C(4)–C(4′) and the low torsion angle at C(3)–C(3′) is illustrated by the pronounced twisting in the C(1)–C(1′) double bond [*e.g.* C(2)–C(1)–C(1′)–C(2′), −8.6(5)°]. This bond is also marginally lengthened by the twisting motion [C(1)–C(1′) in (**4**) is 1.322(4) Å, *cf.* 1.299(9) Å in (**3**)].

The conversion of (**3**) to (**4**) may therefore be considered to proceed by reduction of the $Fe(CO)_3(\eta^5$-dienyl) systems, leading to uncoupling of the terminal contact carbons of the dienyl units [*i.e.* C(4) and C(4′)], followed by C_6 ring inversion and formation of the C(4)–C(4′) bond and with it the cyclobutane ring [C(3),C(3′),C(4),C(4′)]. Oxidation of (**4**) regenerates (**3**) by cleavage of the long, strained C(4)–C(4′) bond. As for the reaction of (**2**) to (**3**), that of (**4**) to (**3**) may be considered to involve electrophilic attack by a cationic 17-electron iron centre on a saturated carbon atom [C(4)], which proceeds with inversion of configuration [at C(4)] and cleavage of the C(4)–C(4′) bond. The specific nature of the interconversion of (**3**) and (**4**) prompts consideration of other reaction paths which might be envisaged. For example, reduction of (**3**) does not lead to cleavage of Fe–C(8) [C(8′)] and formation of a bond between C(8) and C(8′). Such a sequence is not possible since C(8) and C(8′) are *transoid* 1,4-substituents on the C_6 ring (see Figure 3) and hence cannot be brought into proximity without inversion of configuration at C(2) and C(2′). Other possibilities include cleavage of Fe–C(8) [C(8′)] and formation of C(1)–C(8) [C(1′)–C(8′)] bonds, *i.e.* reformation of (**2**), presumably disfavoured since it results in two cyclopropane rings rather than one cyclobutane ring.

Other possible reactions on oxidation of (**4**) can likewise be seen to be unfavourable. Thus electrophilic attack on C(2) [C(2′)] rather than C(4) [C(4′)] would have to result in cleavage of C(2)–C(1) [C(2)–C(1′)] with expulsion of HCCH (!) and retention of the strained C_4 ring.

In the case of (**4**) it is clear that the C–C bond cleaved on oxidation is the longest and presumably the weakest such bond in the hydrocarbon skeleton. Similarly, although with reduced statistical significance it is the longest cyclopropane ring bonds

Table 4. Bond lengths and angles for (4)

Bond lengths (Å)

Fe(1)–C(5)	2.152(3)	Fe(1)–C(8)	2.123(3)	C(4)–C(4′)	1.596(4)	C(9)–O(9)	1.129(5)
Fe(1)–C(7)	2.051(3)	Fe(1)–C(10)	1.800(3)	C(5)–C(6)	1.427(4)	C(11)–O(11)	1.138(4)
Fe(1)–C(9)	1.803(4)	Fe(2)–C(5′)	2.148(3)	C(6)–C(7)	1.392(4)	C(2′)–C(8′)	1.515(4)
Fe(1)–C(11)	1.785(3)	Fe(2)–C(7′)	2.058(3)	C(7)–C(8)	1.423(4)	C(3′)–C(4′)	1.537(4)
Fe(2)–C(6′)	2.053(3)	Fe(2)–C(12)	1.795(4)	C(10)–O(10)	1.122(4)	C(4′)–C(5′)	1.512(4)
Fe(2)–C(8′)	2.138(3)	Fe(2)–C(14)	1.811(3)	C(1′)–C(2′)	1.529(4)	C(5′)–C(6′)	1.420(4)
Fe(2)–C(13)	1.795(4)	C(1)–C(1′)	1.322(4)	C(2′)–C(3′)	1.497(4)	C(6′)–C(7′)	1.413(4)
C(1)–C(2)	1.523(4)	C(2)–C(3)	1.496(4)	C(12)–O(12)	1.120(5)	C(7′)–C(8′)	1.425(4)
C(2)–C(8)	1.520(4)	C(3)–C(3′)	1.531(4)	C(14)–O(14)	1.130(4)	C(13)–O(13)	1.133(4)
C(3)–C(4)	1.543(4)	C(4)–C(5)	1.508(4)	Fe(1)–C(6)	2.059(3)		

Bond angles (°)

C(5)–Fe(1)–C(6)	39.5(1)	C(5)–Fe(1)–C(7)	71.8(1)	C(2)–C(3)–C(4)	128.8(2)	C(2)–C(3)–C(3′)	112.2(2)
C(6)–Fe(1)–C(7)	39.6(1)	C(5)–Fe(1)–C(8)	85.6(1)	C(4)–C(3)–C(3′)	87.9(2)	C(3)–C(4)–C(5)	116.3(2)
C(6)–Fe(1)–C(8)	72.2(1)	C(7)–Fe(1)–C(8)	39.8(1)	C(3)–C(4)–C(4′)	86.4(2)	C(5)–C(4)–C(4′)	113.7(2)
C(5)–Fe(1)–C(9)	92.4(1)	C(6)–Fe(1)–C(9)	94.8(1)	Fe(1)–C(5)–C(4)	117.3(2)	Fe(1)–C(5)–C(6)	66.7(1)
C(7)–Fe(1)–C(9)	122.5(1)	C(8)–Fe(1)–C(9)	161.7(1)	C(4)–C(5)–C(6)	128.1(3)	Fe(1)–C(6)–C(5)	73.7(2)
C(5)–Fe(1)–C(10)	169.7(1)	C(6)–Fe(1)–C(10)	130.5(1)	Fe(1)–C(6)–C(7)	69.9(2)	C(5)–C(6)–C(7)	122.0(3)
C(7)–Fe(1)–C(10)	98.3(1)	C(8)–Fe(1)–C(10)	88.2(1)	Fe(1)–C(7)–C(6)	70.5(2)	Fe(1)–C(7)–C(8)	72.8(2)
C(9)–Fe(1)–C(10)	91.0(2)	C(5)–Fe(1)–C(11)	88.5(1)	C(6)–C(7)–C(8)	122.2(3)	Fe(1)–C(8)–C(2)	117.3(2)
C(6)–Fe(1)–C(11)	126.0(1)	C(7)–Fe(1)–C(11)	130.7(1)	Fe(1)–C(8)–C(7)	67.3(2)	C(2)–C(8)–C(7)	128.5(2)
C(8)–Fe(1)–C(11)	95.7(1)	C(9)–Fe(1)–C(11)	102.4(2)	Fe(1)–C(9)–O(9)	178.1(3)	Fe(1)–C(10)–O(10)	177.2(3)
C(10)–Fe(1)–C(11)	100.3(1)	C(5′)–Fe(2)–C(6′)	39.4(1)	Fe(1)–C(11)–O(11)	176.2(3)	C(1)–C(1′)–C(2′)	126.0(3)
C(5′)–Fe(2)–C(7′)	72.2(1)	C(6′)–Fe(2)–C(7′)	40.2(1)	C(1′)–C(2′)–C(3′)	104.6(2)	C(1′)–C(2′)–C(8′)	112.0(3)
C(5′)–Fe(2)–C(8′)	85.4(1)	C(6′)–Fe(2)–C(8′)	72.3(1)	C(3′)–C(2′)–C(8′)	116.7(2)	C(3)–C(3′)–C(2′)	112.6(2)
C(7′)–Fe(2)–C(8′)	39.7(1)	C(5′)–Fe(2)–C(12)	91.4(1)	C(3)–C(3′)–C(4′)	89.0(2)	C(2′)–C(3′)–C(4′)	128.4(2)
C(6′)–Fe(2)–C(12)	128.4(1)	C(7′)–Fe(2)–C(12)	130.7(1)	C(4)–C(4′)–C(3′)	85.9(2)	C(4)–C(4′)–C(5′)	113.2(2)
C(8′)–Fe(2)–C(12)	94.5(1)	C(5′)–Fe(2)–C(13)	166.5(1)	C(3′)–C(4′)–C(5′)	115.9(2)	Fe(2)–C(5′)–C(4′)	118.1(2)
C(6′)–Fe(2)–C(13)	127.2(1)	C(7′)–Fe(2)–C(13)	95.3(1)	Fe(2)–C(5′)–C(6′)	66.7(2)	C(4′)–C(5′)–C(6′)	128.0(3)
C(8′)–Fe(2)–C(13)	88.0(1)	C(12)–Fe(2)–C(13)	100.9(2)	Fe(2)–C(6′)–C(5′)	73.9(2)	Fe(2)–C(6′)–C(7′)	70.1(2)
C(5′)–Fe(2)–C(14)	92.0(1)	C(6′)–Fe(2)–C(14)	94.0(1)	C(5′)–C(6′)–C(7′)	122.2(3)	Fe(2)–C(7′)–C(6′)	69.7(2)
C(7′)–Fe(2)–C(14)	122.0(1)	C(8′)–Fe(2)–C(14)	161.2(1)	Fe(2)–C(7′)–C(8′)	73.2(2)	C(6′)–C(7′)–C(8′)	121.2(3)
C(12)–Fe(2)–C(14)	104.3(2)	C(13)–Fe(2)–C(14)	90.4(1)	Fe(2)–C(8′)–C(2′)	117.9(2)	Fe(2)–C(8′)–C(7′)	67.1(2)
C(2)–C(1)–C(1′)	126.1(3)	C(1)–C(2)–C(3)	104.6(2)	C(2′)–C(8′)–C(7′)	127.8(2)	Fe(2)–C(12)–O(12)	177.6(3)
C(1)–C(2)–C(8)	113.1(2)	C(3)–C(2)–C(8)	116.3(2)	Fe(2)–C(13)–O(13)	178.1(3)	Fe(2)–C(14)–O(14)	177.6(3)

in (2) and in $[Fe_2(CO)_6(\eta^4:\eta'^4\text{-}C_{16}H_{18})]$ [2] which are cleaved on oxidation. It is also clear, however, that the ring cleavage occurs at the C–C bond which lies opposite the incoming electrophilic iron centre. The stereo- and regio-specificity of these reactions can be seen to result from the requirements for co-ordinative saturation at the iron atoms and for minimisation of conformational and angular strain energies in the hydrocarbon skeleton.

Reactions of Complexes (3) *and* (4).—By comparison with the reactions of (1) with nucleophiles, which result in hydrocarbon ring rearrangement,[4,12] complex (3) and PPh_3 or iodide ion give simple products more similar to those observed with mononuclear tricarbonyl(dienyl)iron cations.

In CH_2Cl_2, a suspension of (3) reacts with two equivalents of PPh_3 to give a yellow solution from which the crystalline bis(phosphonium) salt $[Fe_2(CO)_6\{\eta^4:\eta'^4\text{-}C_{16}H_{16}(PPh_3)_2\}][PF_6]_2$ (5) (Scheme) can be isolated in high yield (Table 1). The ^1H n.m.r. spectrum of (5) (Table 2) shows that nucleophilic attack by the phosphorus ligands occurs at the terminal carbon atoms of the two pentadienyl moieties of (3). The assignment of the spectrum, given in Table 2, is based on PPh_3 addition to C(4) and C(4′), although reaction at C(8) and C(8′) cannot be ruled out.

Iodide ions react with (3) in CH_2Cl_2 to give moderate yields of the neutral di-iodide (6) in which nucleophilic attack at the metal results in carbonyl displacement. The ^1H n.m.r. spectrum of (6) (Table 2) is very similar to that of (3), apart from the shift to low field on carbonyl substitution. However, the room-temperature ^{13}C n.m.r. spectrum of (6) is somewhat different from that of (3) in that resonances due to carbon atoms C(4), C(5), C(7), and C(8) (Scheme) are broadened. More detailed studies on $[Fe_2I_2(CO)_4(\eta^5:\eta'^5\text{-}C_{16}H_{16})]$ have shown [2] that such broadening is due to rotational isomerism, involving the position of the iodide and two carbonyl ligands in relation to the unsymmetrical η^5-bonded pentadienyl group.

Conclusions

The synthesis of (3) and (4) completes a series of reactions in which $[Fe(CO)_3(\eta^4\text{-cot})]$ is converted, *via* electron-transfer reactions, to complexes containing four different $C_{16}H_{16}$ hydrocarbons. The stereo- and regio-specificity of each step further underlines the synthetic potential of organometallic electrochemistry.

Experimental

The preparation, purification, and reactions of the complexes described were carried out under an atmosphere of dry nitrogen. Where appropriate, reactions were monitored by i.r. spectroscopy; unless stated otherwise the complexes are moderately air-stable in the solid state, and dissolve in polar solvents such as CH_2Cl_2 and acetone to give solutions which slowly decompose in air. The complexes $[Fe_2(CO)_6(\eta^5:\eta'^5\text{-}C_{16}H_{16})][PF_6]_2$ (1; L = CO) [4] and $[Fe(\eta\text{-}C_5H_5)_2][PF_6]$ [13] were pre-

Table 5. Torsion angles (°)* for (3)·CH_3NO_2 and (4)

	(3)	(4)
C(1′)–C(1)–C(2)–C(3)	5.4(8) [18.3(8)]	−10.8(4) [−9.6(4)]
C(1′)–C(1)–C(2)–C(8)	129.7(6) [141.8(6)]	116.7(3) [117.8(3)]
C(2)–C(1)–C(1′)–C(2′)	1.0(10)	−8.6(5)
C(1)–C(2)–C(3)–C(4)	93.4(5) [82.6(5)]	153.2(3) [153.7(3)]
C(1)–C(2)–C(3)–C(3′)	−30.2(6) [−42.7(6)]	47.1(3) [46.0(3)]
C(8)–C(2)–C(3)–C(4)	−29.2(7) [−41.4(6)]	27.8(4) [29.3(4)]
C(8)–C(2)–C(3)–C(3′)	−152.8(5) [−166.7(5)]	−78.4(3) [−78.5(3)]
C(1)–C(2)–C(8)–C(7)	−43.7(7) [−32.5(8)]	−89.7(3) [−88.4(4)]
C(3)–C(2)–C(8)–C(7)	81.4(7) [91.0(7)]	31.4(4) [32.2(4)]
C(2)–C(3)–C(4)–C(5)	−38.1(8) [−27.3(8)]	−26.7(4) [−29.0(4)]
C(2)–C(3)–C(4)–C(4′)		−141.4(3) [−142.8(3)]
C(3′)–C(3)–C(4)–C(5)	88.3(7) [99.8(6)]	90.5(2) [89.4(2)]
C(3′)–C(3)–C(4)–C(4′)		−24.3(2) [−24.4(2)]
C(2)–C(3)–C(3′)–C(2′)	50.8(6)	−71.7(3)
C(2)–C(3)–C(3′)–C(4′)	−74.4(5) [−75.1(5)]	156.7(2) [156.9(2)]
C(4)–C(3)–C(3′)–C(4′)	159.7(4)	25.2(2)
C(3)–C(4)–C(5)–C(6)	50.0(9) [48.0(9)]	−33.4(4) [−32.5(4)]
C(4′)–C(4)–C(5)–C(6)		64.7(4) [64.4(4)]
C(3)–C(4)–C(4′)–C(3′)		24.2(2)
C(3)–C(4)–C(4′)–C(5′)		−92.2(3) [−93.0(2)]
C(5)–C(4)–C(4′)–C(5′)		150.6(2)
C(4)–C(5)–C(6)–C(7)	2.8(10) [−0.4(8)]	54.5(4) [55.2(4)]
C(5)–C(6)–C(7)–C(8)	−10.4(10) [−8.3(8)]	0.8(4) [0.6(4)
C(6)–C(7)–C(8)–C(2)	−47.5(8) [−48.4(8)]	−54.9(4) [−55.8(4)]
H(1)–C(1)–C(2)–H(2)	66.3(39) [79.4(47)]	47.7(27) [48.7(27)]

* The corresponding value for the given geometric parameter replacing primed atom labels with unprimed (and *vice versa*) is given in square brackets.

pared by the published methods; the compound K[BH(CHMeEt)$_3$] was purchased from the Aldrich Chemical Company Ltd. Electrochemical studies were carried out as previously described.[14]

Infrared spectra were recorded on Nicolet MX-1 FT or Perkin-Elmer PE 257 instruments and calibrated against the absorption band of polystyrene at 1 601 cm^{-1}. Hydrogen-1 n.m.r. spectra were recorded on a JEOL FX 200 spectrometer, and ^{13}C n.m.r. spectra on JEOL FX 200 or FX 90Q instruments; both were calibrated against $SiMe_4$ as internal reference. Mass spectra were recorded on an AEI MS902 instrument. Microanalyses were by the staff of the Microanalytical Service of the School of Chemistry, University of Bristol. Melting points are uncorrected.

Synthesis of [$Fe_2(CO)_6(\eta^4:\eta'^4$-$C_{16}H_{16})$] (**2**).—To a cold (−78 °C) stirred suspension of [$Fe_2(CO)_6(\eta^5:\eta'^5$-$C_{16}H_{16})$][$PF_6$]$_2$ (**1**; L = CO) (1.38 g, 1.8 mmol) in thf (50 cm^3) was added K[BH(CHMeEt)$_3$] (4 cm^3 of a 1 mol dm^{-3} solution in thf, 4.0 mmol). After 1.5 h the red solution was warmed to room temperature and evaporated to dryness. Extraction of the orange residue with CH_2Cl_2 (15 cm^3) and chromatography on a silica–n-hexane column (40 cm × 3 cm) gave a yellow band which was eluted with n-hexane–diethyl ether (10:1). Evaporation to dryness and recrystallisation from CH_2Cl_2–n-hexane gave the product as yellow crystals, yield 0.15 g (20%).

Preparation of [$Fe_2(CO)_6(\eta^5:\eta'^5$-$C_{16}H_{16})$][$PF_6$]$_2$ (**3**).—To a stirred solution of [$Fe_2(CO)_6(\eta^4:\eta'^4$-$C_{16}H_{16})$] (**2**) (0.35 g, 0.7 mmol) in CH_2Cl_2 (100 cm^3) was added [Fe(η-C_5H_5)$_2$][PF_6] (0.45 g, 1.4 mmol). After 1 h, the white precipitate was filtered off and washed with diethyl ether. Recrystallisation from nitromethane–diethyl ether gave the product, (**3**)·CH_3NO_2, as a pale yellow solid, yield 0.47 g (78%). The product is insoluble in CH_2Cl_2 but soluble in CH_3NO_2 and acetone.

Preparation of [$Fe_2(CO)_6(\eta^4:\eta'^4$-$C_{16}H_{16})$] (**4**).—To a cold (−78 °C) stirred suspension of [$Fe_2(CO)_6(\eta^5:\eta'^5$-$C_{16}H_{16})$][$PF_6$]$_2$·$CH_3NO_2$ (0.42 g, 0.54 mmol) in thf (75 cm^3) was added K[BH(CHMeEt)$_3$] (1.2 cm^3 of a 1 mol dm^{-3} solution in thf, 1.20 mmol). After 1 h, the orange solution was warmed to room temperature and evaporated to dryness. Extraction of the orange residue into CH_2Cl_2 (10 cm^3) and chromatography on an alumina–n-hexane column (20 cm × 2.5 cm), gave a yellow band which was eluted with n-hexane. Evaporation to dryness gave the product as yellow crystals, yield 0.053 g (20%).

Oxidation of [$Fe_2(CO)_6(\eta^4:\eta'^4$-$C_{16}H_{16})$] (**4**) *with Ferrocenium Ion.*—To a stirred solution of [$Fe_2(CO)_6(\eta^4:\eta'^4$-$C_{16}H_{16})$] (**4**) (0.020 g, 0.04 mmol) in CH_2Cl_2 (20 cm^3), was added [Fe(η-C_5H_5)$_2$][PF_6] (0.028 g, 0.08 mmol). After 1 h, the white precipitate was filtered off and washed with diethyl ether to give [$Fe_2(CO)_6(\eta^5:\eta'^5$-$C_{16}H_{16})$][$PF_6$]$_2$ (**3**) as a white solid, yield 0.028 g (88%).

Preparation of [$Fe_2(CO)_6\{\eta^4:\eta'^4$-$C_{16}H_{16}(PPh_3)_2\}$][$PF_6$]$_2$ (**5**).—Solid PPh_3 (0.06 g, 0.23 mmol) was added to a stirred suspension of (**3**)·CH_3NO_2 (0.1 g, 0.13 mmol), in CH_2Cl_2 (20 cm^3). After 3.5 h the yellow solution was filtered and evaporated to low volume. Addition of diethyl ether gave the product, (**5**)·CH_2Cl_2, as a pale yellow solid, yield 0.11 g (72%).

Preparation of [$Fe_2I_2(CO)_4(\eta^5:\eta'^5$-$C_{16}H_{16})$] (**6**).—Solid [$PMePh_3$]I (0.05 g, 0.12 mmol) was added to a yellow suspension of (**3**)·CH_3NO_2 (0.05 g, 0.06 mmol) in CH_2Cl_2 (20 cm^3). After stirring for 1 h, the red solution was filtered, evaporated to dryness, and the residue extracted into toluene (100 cm^3). After removal of toluene *in vacuo*, recrystallisation from dichloromethane–n-hexane yielded the product as a red-brown solid, yield 0.02 g (52%).

Crystal Structure Analyses of (**3**)·CH_3NO_2 *and* (**4**).—Crystals of (**3**)·CH_3NO_2 grow as thin yellow needles from nitromethane–diethyl ether solution. A fragment of dimensions 0.7 × 0.13 × 0.13 mm was cut from a larger crystal and glued in a thin-walled glass capillary under N_2 for structure analysis. Intensity data

Table 6. Atomic co-ordinates ($\times 10^4$) for (**3**)·CH_3NO_2

Atom	*x*	*y*	*z*	Atom	*x*	*y*	*z*
Fe(1)	17 028(1)	5 340(1)	3 671(1)	C(13)	13 126(11)	6 829(3)	−140(2)
Fe(2)	12 824(1)	6 534(1)	573(1)	O(13)	13 356(10)	7 035(3)	−571(2)
C(1)	15 635(9)	7 155(3)	2 620(2)	C(14)	10 363(9)	6 353(3)	235(3)
C(2)	14 750(8)	6 525(3)	2 840(2)	O(14)	8 826(7)	6 226(3)	45(2)
C(3)	14 775(7)	5 856(3)	2 469(2)	P(1)	13 208(2)	6 624(1)	4 913(1)
C(4)	16 453(9)	5 391(3)	2 713(2)	F(1)	15 190(5)	6 864(3)	4 839(2)
C(5)	18 286(8)	5 582(3)	2 973(2)	F(2)	13 267(6)	7 247(3)	5 372(2)
C(6)	18 858(10)	6 081(4)	3 434(3)	F(3)	14 157(7)	6 125(3)	5 442(2)
C(7)	17 638(10)	6 428(3)	3 709(2)	F(4)	12 271(7)	7 096(3)	4 372(2)
C(8)	15 734(9)	6 400(3)	3 494(2)	F(5)	13 173(6)	5 986(2)	4 463(2)
C(9)	14 691(9)	4 995(3)	3 578(2)	F(6)	11 229(5)	6 375(3)	4 986(2)
O(9)	13 202(6)	4 795(3)	3 515(2)	P(2)	9 456(3)	4 493(1)	1 499(1)
C(10)	17 572(9)	5 386(3)	4 481(2)	F(7)	9 812(8)	3 679(2)	1 422(3)
O(10)	17 905(7)	5 412(2)	4 980(2)	F(8)	9 113(9)	5 291(3)	1 589(4)
C(11)	18 220(10)	4 486(4)	3 712(3)	F(9)[a]	7 592(15)	4 406(7)	1 679(5)
O(11)	19 014(9)	3 971(3)	3 720(2)	F(10)[a]	11 228(24)	4 645(7)	1 277(9)
C(1′)	16 237(9)	7 168(3)	2 139(3)	F(11)[a]	10 529(19)	4 678(11)	2 098(5)
C(2′)	16 122(7)	6 556(3)	1 713(2)	F(12)[a]	8 299(18)	4 420(6)	815(4)
C(3′)	14 695(8)	6 017(3)	1 802(2)	F(13)[b]	7 394(12)	4 394(5)	1 279(7)
C(4′)	12 769(7)	6 243(3)	1 480(2)	F(14)[b]	9 389(22)	4 203(6)	2 135(5)
C(5′)	12 044(8)	6 938(3)	1 326(2)	F(15)[b]	11 659(12)	4 595(5)	1 744(6)
C(6′)	12 847(9)	7 481(3)	1 055(2)	F(16)[b]	9 778(19)	4 742(7)	928(4)
C(7′)	14 553(10)	7 409(3)	897(2)	C	4 347(14)	3 232(5)	1 730(4)
C(8′)	15 673(8)	6 813(3)	1 072(2)	N(1)	4 509(10)	3 102(5)	2 370(4)
C(12)	13 548(9)	5 618(4)	507(2)	O(1)	4 125(11)	2 514(6)	2 493(4)
O(12)	13 986(8)	5 044(3)	473(2)	O(2)	5 137(12)	3 564(5)	2 709(3)

[a] Occupancy 0.457(6). [b] Occupancy 0.543(6).

Table 7. Atomic co-ordinates ($\times 10^4$) for (**4**)

Atom	*x*	*y*	*z*	Atom	*x*	*y*	*z*
Fe(1)	3 219(1)	8 299(1)	7 010(1)	O(11)	4 067(2)	6 484(2)	5 997(2)
Fe(2)	8 933(1)	7 761(1)	9 929(1)	C(1′)	7 303(3)	9 891(2)	7 295(3)
C(1)	6 425(3)	9 715(2)	6 579(2)	C(2′)	7 557(2)	9 395(2)	8 402(2)
C(2)	5 562(2)	8 881(2)	6 647(2)	C(3′)	6 529(2)	8 846(2)	8 540(2)
C(3)	6 040(2)	8 197(2)	7 564(2)	C(4′)	6 388(2)	7 887(2)	9 242(2)
C(4)	5 451(2)	7 527(2)	8 301(2)	C(5′)	7 333(2)	7 125(2)	9 437(2)
C(5)	4 333(2)	7 897(2)	8 431(2)	C(6′)	8 066(2)	6 861(2)	8 741(2)
C(6)	3 939(2)	8 956(2)	8 432(2)	C(7′)	8 671(2)	7 636(3)	8 298(2)
C(7)	4 002(2)	9 652(2)	7 600(2)	C(8′)	8 578(2)	8 728(2)	8 540(2)
C(8)	4 450(2)	9 349(2)	6 691(2)	C(12)	8 433(3)	8 702(3)	10 781(3)
C(9)	2 076(3)	7 762(3)	7 527(3)	O(12)	8 094(3)	9 300(3)	11 284(2)
O(9)	1 347(2)	7 419(3)	7 823(3)	C(13)	10 325(3)	8 170(3)	10 045(3)
C(10)	2 326(3)	8 875(3)	5 903(3)	O(13)	11 194(2)	8 456(3)	10 109(3)
O(10)	1 801(2)	9 227(2)	5 188(2)	C(14)	9 341(3)	6 638(3)	10 783(2)
C(11)	3 702(3)	7 180(2)	6 378(2)	O(14)	9 629(2)	5 938(2)	11 304(2)

for a quadrant of reciprocal space were collected in the range $4 < 2\theta < 50°$ on a Nicolet *P3m* diffractometer at room temperature. For reflections with $2\theta > 40°$ only those with raw intensity > 25 counts in a 2-s prescan were collected. Integrated intensities were measured by the θ—2θ method with scan widths $(2.4 + \Delta\alpha_1\alpha_2)°$ and speeds varying between 2.0 and 29.3° min^{-1}. Three check reflections (1 $\bar{8}$ $\bar{4}$, 4 $\bar{4}$ $\bar{7}$, $\bar{2}$ 0 12) were remeasured after every 50 reflections and showed no significant variation during the experiment. A numerical absorption correction based on the indexed crystal faces was applied to the 4 644 intensity data collected; maximum and minimum transmission coefficients were 0.870 and 0.796, respectively. 4 054 Unique data remained after averaging of duplicate and symmetry related measurements and deletion of systematic absences; of these 3 242 with $I > 1.5\sigma(I)$ were used in the structure solution and refinement.

Crystal data for (**3**)·CH_3NO_2·$C_{22}H_{16}F_{12}Fe_2O_6P_2$·$CH_3NO_2$, M = 840.9, monoclinic, a = 7.353(3), b = 18.706(10), c = 23.205(15) Å, β = 104.06(4)°, U = 3 095(3) Å^3, Z = 4, D_c = 1.80 g cm^{-3}, $F(000)$ = 1 680 electrons, space group $P2_1/n$ (non-standard setting of no. 14, $P2_1/c$), Mo-K_α X-radiation, graphite monochromator, $\bar{\lambda}$ = 0.710 69 Å, μ(Mo-K_α) = 11.44 cm^{-1}, T = 295 K, crystal faces [distance from origin (mm)]: (0 0 1) [0.10], (0 0 $\bar{1}$) [0.10], (0 1 $\bar{1}$) [0.06], (0 $\bar{1}$ 1) [0.06], (0 $\bar{1}$ $\bar{1}$) [0.09], (0 1 1) [0.09], (1 0 0) [0.35], ($\bar{1}$ 0 0) [0.35].

Data collection and reduction for (**4**) proceeded in a similar fashion as for (**3**)·CH_3NO_2 with the following exceptions. Yellow-green plate-like crystals of (**4**) were grown from n-hexane solution at −20 °C. Crystal dimensions were *ca.* 0.8 × 0.65 × 0.13 mm. Three check reflections (5 0 0, 0 6 0, and 0 0 6) were remeasured after every 100 reflections; $2\theta_{max.}$ was 50° with all reflections collected after the prescan. The transmission coefficients for the 4 950 reflections collected varied between 0.797 and 0.348; data reduction gave 4 462 unique observations of which 3 878 with $I > 1.5\sigma(I)$ were used.

Crystal data for (**4**). $C_{22}H_{16}Fe_2O_6$, M = 487.9, monoclinic, a = 12.489(5), b = 12.655(5), c = 12.768(5) Å, β = 99.74(4)°, U = 1 988(1) Å^3, Z = 4, D_c = 1.63 g cm^{-3}, $F(000)$ = 992, space

group $P2_1/c$ (no. 14), Mo-K_α X-radiation, graphite monochromator, $\bar{\lambda} = 0.710\,69$ Å, μ(Mo-K_α) = 14.94 cm^{-1}, $T = 295$ K, crystal faces [distances from origin (mm)]: (1 0 0) [0.075], ($\bar{1}$ 0 0) [0.075], (0 1 1) [0.35], (0 $\bar{1}$ $\bar{1}$) [0.35], (0 1 $\bar{1}$) [0.425], (0 $\bar{1}$ 1) [0.425].

Structure solution and refinement. The structures were solved by orthodox heavy-atom methods, all atoms including hydrogen being located directly. Refinement was by blocked-cascade full-matrix least squares with all non-hydrogen atoms being assigned anisotropic vibrational parameters, and hydrogen atoms isotropic parameters. In the case of (**3**)·CH_3NO_2, one $[PF_6]^-$ anion showed disorder in having two sites for a set of four (coplanar) fluorine atoms. The occupancies of these sites were refined to 0.457(6) and 0.543(6), respectively. Individual reflections were assigned weights $w = [\sigma^2(F_o) + gF_o^2]^{-1}$ [$\sigma^2(F_o)$ = variance due to counting statistics, $g = 0.0007$ for (**3**)·CH_3NO_2 and $g = 0.0005$ for (**4**)]. Refinement converged to final residuals $R = 0.0543$, $R' = 0.0536$, and $S = 1.33$ for (**3**)·CH_3NO_2 and $R = 0.0541$, $R' = 0.0531$, $S = 1.85$ for (**4**).* Final difference electron-density maps showed features of magnitude < 0.45 e Å^{-3} for (**3**)·CH_3NO_2, the largest being near the disordered $[PF_6]^-$ anion; for (**4**) the corresponding value was 0.69 e Å^{-3}, the peaks being near the metal atoms. Non-hydrogen atom positional parameters for (**3**)·CH_3NO_2 and (**4**) are given in Tables 6 and 7, respectively. Complex neutral-atom scattering factors were taken from ref. 15, and all calculations carried out with programs of the SHELXTL package.[16] The crystal structure of (**3**)·CH_3NO_2 consists of isolated $[Fe_2(CO)_6(\eta^5:\eta'^5\text{-}C_{16}H_{16})]^{2+}$ dications, $[PF_6]^-$ anions, and CH_3NO_2 molecules of solvation, separated by normal non-bonded distances. The structure of (**4**) is likewise composed of isolated molecules separated by typical van der Waals distances.

Acknowledgements

We thank the S.E.R.C. for a Research Studentship (to J. B. S.) and a Postdoctoral Research Assistantship (to M. W. W.). We also thank Drs. R. J. Goodfellow and M. Murray for invaluable assistance with n.m.r. spectroscopy, and Professor B. R. Penfold for the atomic positional parameters of complex (**2**).

* $R = \Sigma||F_o| - |F_c||/\Sigma|F_o|$; $R' = \Sigma w^{\frac{1}{2}}||F_o| - |F_c||/\Sigma w^{\frac{1}{2}}|F_o|$; $S = [\Sigma w(|F_o| - |F_c|)^2/(\text{N.O.} - \text{N.V.})]^{\frac{1}{2}}$.

References

1 Part 21, N. G. Connelly, M. J. Freeman, A. G. Orpen, A. R. Sheehan, J. B. Sheridan, and D. A. Sweigart, preceding paper.
2 N. G. Connelly, A. R. Lucy, R. M. Mills, J. B. Sheridan, and P. Woodward, *J. Chem. Soc., Dalton Trans.*, 1985, 699.
3 N. G. Connelly, A. R. Lucy, R. M. Mills, J. B. Sheridan, M. W. Whiteley, and P. Woodward, *J. Chem. Soc., Chem. Commun.*, 1982, 1057.
4 N. G. Connelly, R. L. Kelly, M. D. Kitchen, R. M. Mills, R. F. D. Stansfield, M. W. Whiteley, S. M. Whiting, and P. Woodward, *J. Chem. Soc., Dalton Trans.*, 1981, 1317.
5 H. A. Bockmeulen, R. G. Holloway, A. W. Parkins, and B. R. Penfold, *J. Chem. Soc., Chem. Commun.*, 1976, 298.
6 T. A. Albright, P. Hofmann, and R. Hoffmann, *J. Am. Chem. Soc.*, 1977, **99**, 7546.
7 K. Broadley, N. G. Connelly, R. M. Mills, M. W. Whiteley, and P. Woodward, *J. Chem. Soc., Dalton Trans.*, 1984, 683.
8 J. A. D. Jefferys and C. Metters, *J. Chem. Soc., Dalton Trans.*, 1977, 729.
9 R. P. Dodge, *J. Am. Chem. Soc.*, 1964, **86**, 5429.
10 D. L. Smith and L. F. Dahl, *J. Am. Chem. Soc.*, 1962, **84**, 1743.
11 J. C. J. Bart, P. Piccardi, and I. W. Bassi, *Acta Crystallogr., Sect. B*, 1980, **36**, 842.
12 N. G. Connelly, A. R. Lucy, R. M. Mills, M. W. Whiteley, and P. Woodward, *J. Chem. Soc., Dalton Trans.*, 1984, 161.
13 J. C. Smart and B. L. Pinsky, *J. Am. Chem. Soc.*, 1980, **102**, 1009.
14 N. G. Connelly, M. J. Freeman, I. Manners, and A. G. Orpen, *J. Chem. Soc., Dalton Trans.*, 1984, 2703.
15 'International Tables for X-Ray Crystallography,' Kynoch Press, Birmingham, 1975, vol. 4.
16 G. M. Sheldrick, SHELXTL programs for use with the Nicolet X-Ray System, Cambridge, 1976; updated Göttingen, 1981.

Received 13*th August* 1984; *Paper* 4/1419